THE JOURNAL OF PHYSICAL CHEMISTRY A

A JOURNAL OF THE AMERICAN CHEMICAL SOCIETY

CELEBRATING 125 YEARS

January 28, 2021
Volume 125
Number 3
pubs.acs.org/JPCA

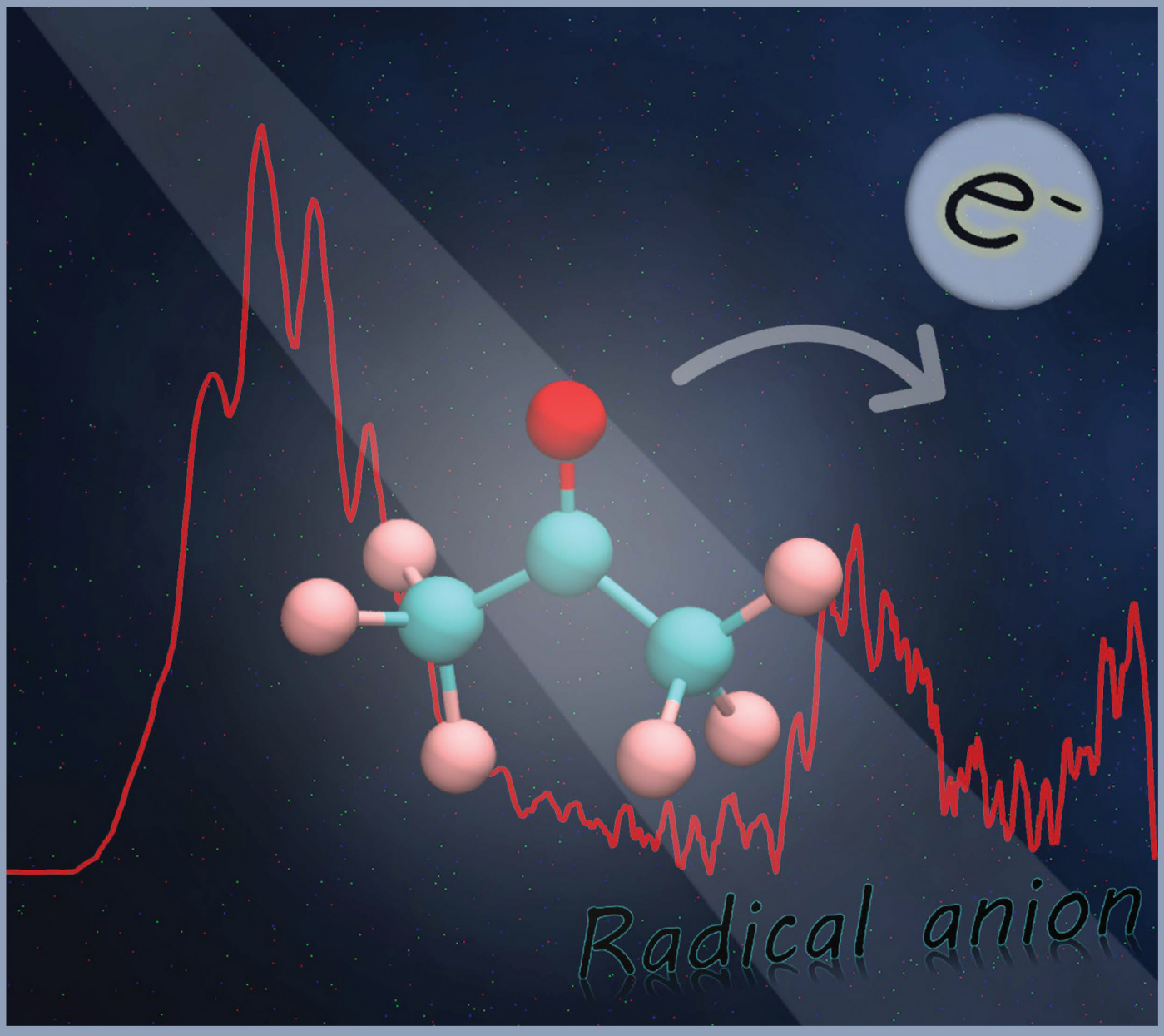

ACS Publications
Most Trusted. Most Cited. Most Read.

www.acs.org

THE JOURNAL OF PHYSICAL CHEMISTRY A

pubs.acs.org/JPCA Article

Electron Affinity and Electronic Structure of Hexafluoroacetone (HFA) Revealed by Photodetaching the $[HFA]^{\bullet-}$ Radical Anion

Lei Wang,[§] Jia Han,[§] Qinqin Yuan, Wenjin Cao, Xiaoguo Zhou,* Shilin Liu, and Xue-Bin Wang*

Cite This: *J. Phys. Chem. A* 2021, 125, 746−753 Read Online

ACCESS | Metrics & More | Article Recommendations | Supporting Information

ABSTRACT: A great deal of effort has been focused on developing a metal-free catalytic system for epoxidation of unreactive alkenes. Fluoroketones are thought as remarkably promising catalysts for epoxidation reactions. The combination of fluorinated alcohols and catalytic amounts of hexafluoroacetone (HFA) gives a versatile and effective medium for epoxidation of various olefins with hydrogen peroxide. However, the fundamental physicochemical properties of HFA remained largely unclear, although they were very important to understand the related interactions. Here, we performed a joint study on the electron affinity and electronic structure of HFA employing negative ion photoelectron (NIPE) spectroscopy and quantum chemistry calculations. Two distinct bands with complicated vibrational progressions were observed in the 193 nm NIPE spectrum. The adiabatic/vertical detachment energies (ADE/VDE) were derived to be 1.42/2.06 and 4.43/4.86 eV for the ground singlet state and excited triplet state, respectively. Using the optimized geometries and vibrational frequencies of the anion and the neutral, the Franck−Condon factors were calculated for electron detachments to produce HFA in its lowest singlet and triplet states. Good agreements are obtained hereby for both bands between the experimental and calculated NIPE spectra, when taking into account combination vibrational excitations, unequivocally revealing that HFA possesses a singlet ground state with a giant singlet−triplet energy difference (ΔE_{ST}). The electron affinity (EA) and ΔE_{ST} of HFA were therefore determined to be EA = 1.42 ± 0.02 eV and ΔE_{ST} = −3.01 eV.

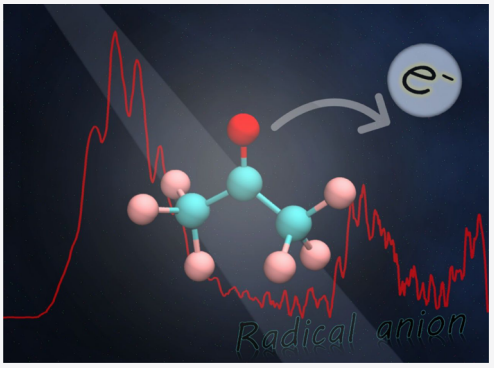

1. INTRODUCTION

Fluorinated compounds have attracted extensive attention in some fields, e.g., organic synthesis, homogeneous catalysis, and biological application.[1−3] Being at the far end of the first row of the periodic table, fluorine is the most electronegative element with a small atom volume. Due to the strong negative inductive effect of fluorine substituents, fluorinated compounds display unique properties distinct from the corresponding non-fluorinated analogues.[4] The beneficial effects of fluorination compared to hydrocarbons, such as high thermal and oxidative stability, low polarity, and weak intermolecular interactions, are increasingly utilized in the pharmaceutical industry and crystal engineering.[5−10] Moreover, fluorine-containing materials have also generated great interest as polymers, reaction media, and catalysts.[11−15]

Hexafluoroacetone (HFA) was first prepared through the direct fluorination of acetone in 1941.[16] Compared with other organic ketones, HFA is highly susceptible to nucleophilic attack resulting from the strong electron-withdrawing effect of the fluorine atoms.[17] This electron-poor carbonyl with low proton affinity was found to be particularly useful in detecting short-lived and highly reactive atmospheric species.[18−20] Using Fourier transform infrared spectroscopy, Horie et al.[21] and Taatjes et al.[22] used HFA as an efficient and clean scavenger of Criegee intermediates to form secondary ozonides. Moreover, since fluorinated ketones are highly soluble in the fluorous phase and can be easily separated from substrates and products without noticeable decomposition, they have been tested as catalysts in a few systems to improve the epoxidation of unreactive substrates.[23,24] The combination of fluorinated alcohols and catalytic amounts of HFA affords an extraordinarily promising medium for epoxidation of usually poorly reactive alkene substrates with aqueous hydrogen peroxide.[25−28] Sheldon et al.[29] reported that the addition of a small amount of HFA greatly accelerated the relative reaction and allowed the epoxidation to proceed at room temperature.

However, the stabilization effect and catalytic mechanism remain obscure due to the lack of gas-phase study of HFA itself. There is relatively little information about the optical investigations in the available literature to date. In 1968, Gandini et al.[30] obtained the fluorescence and phosphorescence emission spectra of HFA vapor excited with 313 nm

Received: October 3, 2020
Revised: November 30, 2020
Published: December 9, 2020

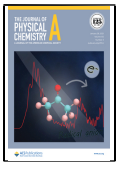

https://dx.doi.org/10.1021/acs.jpca.0c08996
J. Phys. Chem. A 2021, 125, 746−753

Scheme 1. Molecular Structures of HFIP, $[HFIP_{-H}]^-$, and $[HFIP_{-2H}]^{\bullet-}$ (i.e., $HFA^{\bullet-}$)

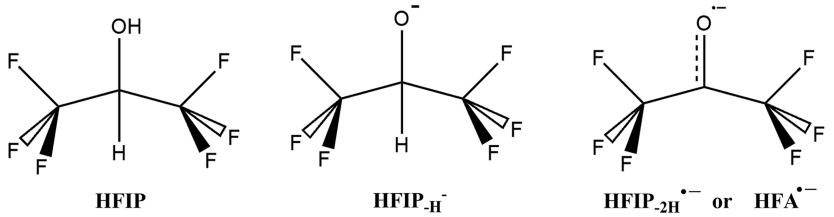

light from a mercury arc lamp. The fluorescence extends to ca. 700 nm with a maximum intensity close to 415 nm, while the phosphorescence band has a maximum at 470 nm, providing approximate vertical excitation energies for the S_1 (2.99 eV) and T_1 (2.64 eV) states. Besides, electron impact experiments showed that the HFA molecule could effectively capture thermal electrons into a temporary parent negative ion state, HFA^-, with an autodetachment lifetime of 65 μs.[31−35] In a gas-phase ion−molecule reaction of the dioxygen radical anion with neutral HFA carried out in a flowing afterglow apparatus, the $HFA^{\bullet-}$ radical anion was observed and the electron affinity (EA) of HFA was estimated to be ca. 33 kcal/mol (1.43 eV).[36] However, there are no reports on direct measurements or computations of EA of HFA to the best of our knowledge. Therefore, given the significance and versatility of HFA, it is desirable to explore the geometries and electronic configurations of HFA and its radical anion.

Negative ion photoelectron (NIPE) spectroscopy is a powerful experimental technique, not only directly yielding adiabatic detachment energy (ADE) of anion but also probing the ground and excited states of the corresponding neutral molecule within detachment photon energy.[37−42] In particular, it is also efficient for investigating the relatively short-lived and reactive radical species.[43−53] In this work, we have performed an experimental and theoretical joint study of the $HFA^{\bullet-}$ radical anion, employing low-temperature NIPE spectroscopy coupled with an electrospray ionization (ESI) source and high-level ab initio theoretical calculations. By photodetaching the $HFA^{\bullet-}$ radical anion in the doublet ground state, either closed-shell singlet or triplet states of the neutral could be produced. Thus, both geometries and electronic configurations of the $HFA^{\bullet-}$ radical anion and the corresponding neutral in lowest singlet and triplet states are revealed from the spectral analyses. The EA of HFA was directly determined for the first time. All of these details provide valuable spectroscopic quantities to help rationalize the catalytic mechanism of fluoroketones in the epoxidation reactions involving fluorinated alcohols.

2. METHODS

2.1. Experimental Section. The NIPE spectra were measured using the magnetic bottle time-of-flight (TOF) photoelectron spectrometer at Pacific Northwest National Laboratory, equipped with an ESI source and a temperature-controlled cryogenic ion trap.[54] The target anions were produced by electrospraying 1×10^{-3} M aqueous methanolic (3:1 volume ratio of methanol and water) solution of hexafluoroisopropanol (HFIP) with the pH value of the solution being adjusted to 9−10 by adding a NaOH aqueous solution dropwise. Interestingly, the weak $[HFIP_{-2H}]^{\bullet-}$ radical anions were produced besides the dominant $[HFIP_{-H}]^-$ anions,[37] presumably via the mechanism of double deportation of HFIP in basic solution to yield the $[HFIP_{-2H}]^{2-}$ dianions, followed by electron autodetachment in the gas phase. Similar mechanisms were proposed in our previous studies of radical anions.[43−45] To make it clear, the molecular structures of HFIP, $[HFIP_{-H}]^-$ anion, and $[HFIP_{-2H}]^{\bullet-}$ radical anion are shown in Scheme 1. Obviously, the $[HFIP_{-2H}]^{\bullet-}$ anion is the so-called $[HFA]^{\bullet-}$ radical anion here, and thus we keep the notation of $[HFA]^{\bullet-}$ instead of $[HFIP_{-2H}]^{\bullet-}$ below for clarity. All anions were transported into vacuum by two RF-only ion guides, accumulated and thermalized at 20 K in a cryogenic 3D trap. The cold anions were then pushed out into the extraction zone of the TOF mass spectrometer at 10 Hz, and the desired $[HFA]^{\bullet-}$ anions were carefully mass-selected and decelerated before being photodetached in the interaction zone with a 193 nm (6.424 eV) laser beam (EX100F, GAM ArF laser). The laser was operated at a 20 Hz repetition rate with the anion beam off at alternating laser shots, enabling shot-by-shot background subtraction. The photodetached electrons were collected with nearly 100% efficiency by a magnetic bottle and analyzed with a 5.2 m long electron flight tube. The recorded TOF photoelectron spectrum was converted into an electron kinetic energy (eKE) spectrum, calibrated with the known transitions of I^- and $Cu(CN)_2^-$. Then, the electron binding energy (EBE) spectrum was obtained by subtracting the kinetic energy spectrum from the detachment photon energy. The electron energy resolution was about 2% (i.e., ~20 meV for electrons with 1 eV kinetic energy).

2.2. Computational Details. To interpret the NIPE spectrum of $[HFA]^{\bullet-}$, geometry optimization and electronic configuration calculations were performed using M06-2X,[55] PBE0,[56] and ωB97XD[57] density functionals with the aug-cc-pVTZ basis set. All of these density functional theory (DFT) calculations were carried out using the Gaussian 16 software package.[58] Using the optimized geometries of the anion and neutral, vibrational frequency analyses were performed at the same level of theory to confirm that minima were found and to compute the zero-point energy (ZPE). The theoretical adiabatic detachment energy (ADE) was calculated as the energy difference between the radical anion and the corresponding neutral at each in its own optimized geometry, with ZPE corrections, while the vertical detachment energy (VDE) was computed as the energy difference between the anion and neutral, both in the optimized anion's structure.

Based on the obtained geometries, vibrational frequencies, normal coordinates of the anion, and the corresponding neutral, Franck−Condon factors (FCFs) were calculated using the ezSpectrum program,[59] in which Duschinsky rotation[60] was included to assess vibrational progressions of each specific electronic transition from the anion ground state to the singlet or triplet state of the neutral. Then, the NIPE spectrum of $[HFA]^{\bullet-}$ was simulated with a certain full width at half-maximum (FWHM), according to the experimental conditions.

https://dx.doi.org/10.1021/acs.jpca.0c08996
J. Phys. Chem. A 2021, 125, 746−753

3. RESULTS AND DISCUSSION

3.1. NIPE Spectrum of $[HFA]^{\bullet-}$. The experimental low-temperature NIPE spectrum of $[HFA]^{\bullet-}$ radical anion at 193 nm is shown in Figure 1. In the spectrum, two transition bands

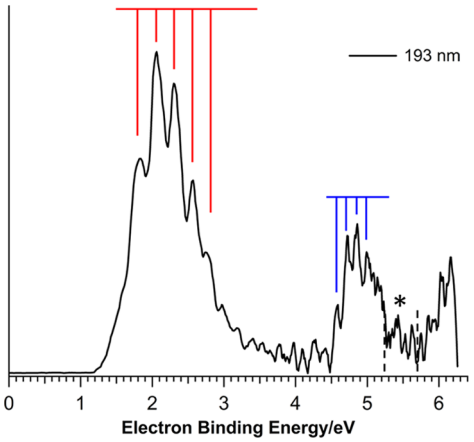

Figure 1. Low-temperature (20 K) photoelectron spectrum of the $[HFA]^{\bullet-}$ radical anion at 193 nm (6.424 eV).

are distinctly observed within the EBE range of 1−6 eV, with centers at 2.06 and 4.86 eV, respectively. Partially resolved vibrational structures can be discerned for these two bands. Since only a unique isomer exists for the $[HFA]^{\bullet-}$ radical anion, we naturally attribute these two bands to two electronic states of the neutral, considering such a large energy gap between them. Thus, the lower energy one is without doubt attributed to the transition to the ground singlet state of the neutral, while the higher one is assigned to the transition to the excited triplet and/or singlet state of the neutral. We will clarify the assignments in the following sections with the aid of high-level ab initio calculations.

As shown in Figure 1, the first band is relatively broad, spanning from 1.3 to 3.5 eV. A vibrational progression with an interval of 1895 ± 50 cm^{-1} is clearly visible, as displayed with red lines. Similarly, the second band covers a relatively narrow EBE range of 4.5−5.2 eV, in which a series of vibrational peaks are also observed with an interval of 1160 ± 50 cm^{-1}. Besides, there is a sharp peak in the 5.2−5.7 eV range (indicated with dotted lines and *) and a rising edge at the EBE of greater than 5.8 eV, indicative of the existence of higher excited states of the neutral, although the signal-to-noise ratio is not good enough to make vibrational assignments. Taking the experimental resolution into account, the ADE and the VDE of the $[HFA]^{\bullet-}$ radical anions can be estimated from the first band onset threshold and maximum in the NIPE spectrum, as 1.42 ± 0.02 eV for ADE and 2.06 ± 0.02 eV for VDE. Similarly, for the second band, the ADE and the VDE are 4.43 ± 0.02 and 4.86 ± 0.02 eV, respectively (Table 1). Apparently, the onset thresholds of both bands are much lower than their peak maximums, with differences of 0.64 and 0.43 eV for the first and second bands, respectively. This implies that the significant geometrical change occurs in the electron photodetachment processes to produce the HFA neutral in both states. In addition, a large energy gap of 3.01 eV (69.4 kcal/mol) exists for these two states.

It is worth noting that the instrument resolutions are about 700 and 225 cm^{-1} for the first and second bands, respectively, at 193 nm. A much better resolved spectrum would have been observed if only one vibrational mode with frequencies of 1895 and 1160 cm^{-1} was involved in each band. The fact that only partially resolved vibrational structures were obtained, particularly in the onset rising edges for both bands, strongly indicates that multiple vibrational modes of the HFA neutral might be excited upon electron photodetachment.

3.2. Geometries and Energetics of the $[HFA]^{\bullet-}$ Anion and HFA Neutral. Figure 2 shows the optimized geometries of $[HFA]^{\bullet-}$ and the corresponding neutral in the ground singlet (S_0) and the lowest triplet (T_1) states at M06-2X, PBE0, and ωB97XD levels of theory with the aug-cc-pVTZ basis set. The corresponding time-dependent density functional theory (TD-DFT) was used to optimize the first electronically excited singlet state (S_1) of neutral HFA, and the ruslts are shown in Figure S1 of the Supporting Information. Apparently, three functional levels show very similar structures. For instance, the C−O bond length of the anion is 1.275 Å at M06-2X and 1.276 Å at both PBE0 and ωB97XD levels, while the relative variations of the dominant C−C bond lengths are less than 0.01 Å at the three levels. Thus, only the M06-2X results are presented for simplicity in the following discussions unless otherwise noted.

In comparison with the anion geometry, the neutral HFA in the ground singlet state shows a few evident variations. The C−O bond length is reduced by 0.091 Å, while the two C−C bonds are elongated by 0.061−0.068 Å. More interestingly, the relative orientation for two CF_3 groups transforms from the staggered form to an eclipsed form in the manner of Newman projection. Somewhat differently, the triplet neutral HFA has a slightly elongated C−O bond (1.306 Å) compared to the anion (1.275 Å). In addition, the C−C−C−F dihedral angle is evidently distorted in the triplet state (140°) from the nearly planar angle (168°) in the anion. Consequently, such geometrical changes strongly imply that the C═O stretching, the carbon skeleton symmetric stretching, and the CF_3 wagging vibrations of neutral HFA would be excited in the electron photodetachment of the anion to produce the neutral in both S_0 and T_1 states. In other words, electron detachment would induce multiple active vibrational modes.

Using these optimized geometries, the ADEs and VDEs of the $[HFA]^{\bullet-}$ radical anion were calculated using M06-2X,

Table 1. Experimental and Calculated Adiabatic Detachment Energies (ADEs) and Vertical Detachment Energies (VDEs) for the $[HFA]^{\bullet-}$ Radical Anion and Excitation Energies of Low-Lying Electronic States of the Corresponding Neutral

	ADE (eV)				VDE (eV)			
state	exp.	M06-2X	PBE0	ωB97XD	exp.	M06-2X	PBE0	ωB97XD
S_0	1.42	1.55	1.51	1.41	2.06	2.31	2.22	2.13
T_1	4.43	4.62	4.30	4.37	4.86	4.94	4.63	4.69
S_1	~5.2	5.02			~5.4	5.29		
ΔE_{ST}	−3.01	−3.07	−2.79	−2.96	−2.80	−2.63	−2.41	−2.56

https://dx.doi.org/10.1021/acs.jpca.0c08996
J. Phys. Chem. A 2021, 125, 746−753

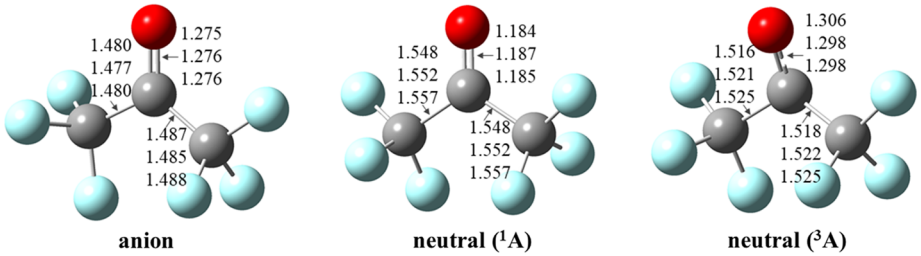

Figure 2. Optimized geometries of the $[HFA]^{\bullet-}$ radical anion and the corresponding neutral HFA in the lowest singlet (S_0) and triplet (T_1) states, calculated at M06-2X, PBE0, and ωB97XD levels of theory with the aug-cc-pVTZ basis set (from top to bottom). Dominant bond lengths are noted in units of Å.

PBE0, and ωb97XD density functional levels. Table 1 summarizes the present experimental and theoretical results. Apparently, all calculated values are in excellent agreement with our experimental results. For instance, ADE and VDE to produce neutral HFA in the S_0 state are calculated to be 1.55 and 2.31 eV, respectively, at the M06-2X level, while those for the triplet neutral (T_1) are 4.62 and 4.94 eV. The energy gap between these two states, ΔE_{ST}, is 3.07 eV for ADE and 2.63 eV for VDE, which are close to the experimental data in Table 1. Therefore, the two bands in the NIPE spectrum are attributed to the electron photodetachment to the ground singlet and lowest triplet states of the neutral. Additionally, the ADE and VDE for neutral HFA in the S_1 state are calculated to be 5.02 and 5.29 eV, respectively. It is worth noting that there are a few weak peaks at the higher EBE side of the T_1 band (denoted with dotted lines and a star in Figure 1), ranging from 5.2 to 5.7 eV, which approximately match the energy for the electronic transition to the first excited singlet state predicted by theoretical calculations. Based on the satisfactory agreement between experimental observations and calculated results, we tentatively assign them as derived from the contribution of the electronic transition to the S_1 state by photodetaching the radical anion.

As shown in Table 1, the M06-2X calculation showed the generally best performance in detachment energy calculations among the three levels, and thus it was subsequently applied for electron configuration analyses. Figure 3 shows the two highest occupied molecular orbitals (HOMO and HOMO-1) of the $[HFA]^{\bullet-}$ radical anion. Open-shell electron configuration analyses provide separately occupied molecular orbital energies of α and β electrons. Apparently, when an electron is detached from different occupied molecular orbitals, different electronic states of the neutral can be produced, and the orbital energies can be used to assess the corresponding EBE.

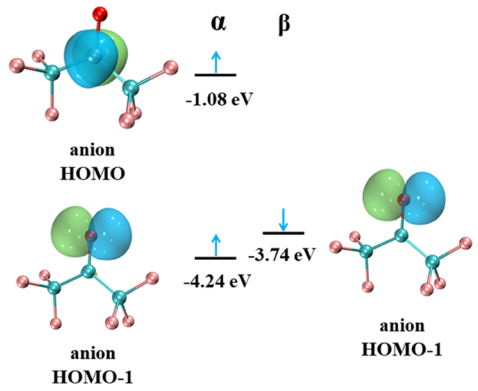

Figure 3. Two highest occupied molecular orbitals (HOMO and HOMO-1) of $[HFA]^{\bullet-}$, as well as their orbital energies, calculated at the M06-2X/aug-cc-pVTZ level of theory.

As displayed in Figure 3, the HOMO of $[HFA]^{\bullet-}$ is located at the central carbon atom with considerable p orbital characteristics. The occupation of low-lying HOMO-1 by two electrons of the carbonyl oxygen atom clearly indicates its significant lone-pair electron features. The orbital energies of β electron HOMO-1 are lower than those of HOMO by 2.66 eV, which is consistent with the experimental energy gap of 2.80 eV. This consistency verifies that the T_1 state of neutral HFA may be produced by the electron detachment from HOMO-1 of the anion.

In contrast to the formation of the triplet neutral HFA, the ground singlet state of the neutral is formed accompanying the detachment of the unpaired electron of HOMO from the radical anion. Consequently, the repulsion between the unpaired electron of HOMO and the lone-pair electrons of the carbonyl oxygen atom disappears upon electron detachment, leading to a shortened C═O bond length in Figure 2. Meanwhile, this unpaired electron removal from HOMO slightly weakens two adjacent σ(C−C) bonds, allowing these C−C bonds to "bounce back" to their original σ bonding status. This inference could also be approved by comparing the C−C bond lengths of the singlet neutral, $[HFA]^{\bullet-}$ and $[HFIP_{-H}]^{-}$ anion. At the same level of theory, the C−C bond lengths were 1.548 Å in HFA (S_0), ∼1.483 Å in $[HFA]^{\bullet-}$, and 1.549 Å in the $[HFIP_{-H}]^{-}$ anion. Apparently, almost identical bond lengths exist in HFA ($HFIP_{-2H}$) (S_0) and the $[HFIP_{-H}]^{-}$ anion, where one σ(C−H) bond is formed for the central carbon atom to consume the HOMO electron. Moreover, for the triplet neutral HFA, the deviation from the nearly planar structure of the anion is attributed to the asymmetric distribution of electron density induced by the loss of one lone-pair of electrons.

3.3. Franck−Condon Factors of the Vibrational Excitation Progressions. Usually, the vibrational structure in the low-temperature NIPE spectrum can reflect the vibrational excitations according to geometry transformation from negative ions to the corresponding neutral, accompanying electron detachments. Accordingly, the FCFs of the transitions from the ground-state radical anion to each electronic state of the neutral were calculated. Figure 4 displays the calculated FCFs of vibrational progressions (in sticks) for detachment of $[HFA]^{\bullet-}$ to the neutral in the S_0 state. As mentioned above, multiple vibrations of neutral HFA might be excited simultaneously in the electron photodetachment, resulting in the fact that combination vibrations should dominantly contribute to the NIPE spectrum in Figure 1.

https://dx.doi.org/10.1021/acs.jpca.0c08996
J. Phys. Chem. A 2021, 125, 746−753

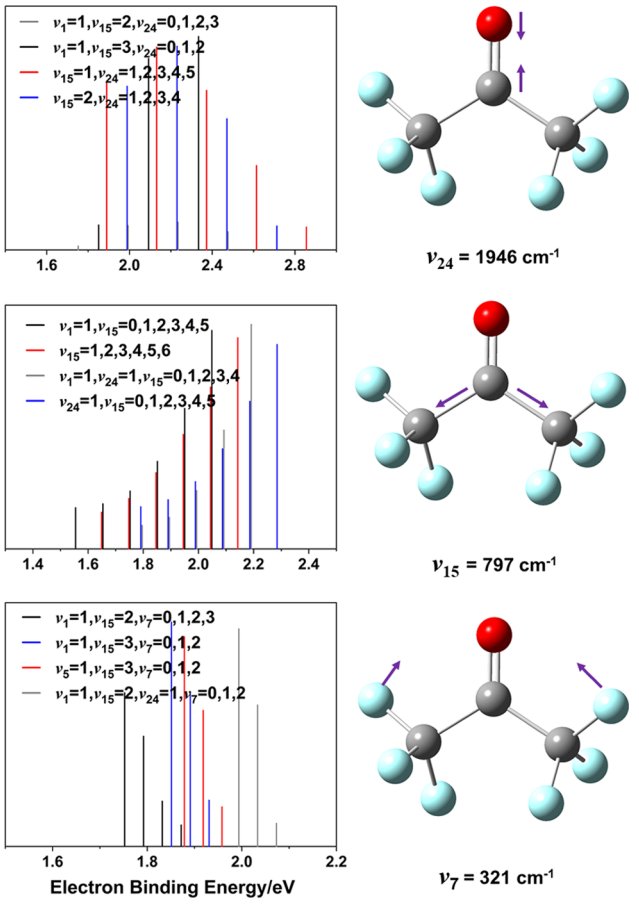

Figure 4. Calculated vibrational progressions (stick spectra) for the Franck−Condon transitions from $[HFA]^{\bullet-}$ to the HFA neutral in the S_0 state, using the optimized geometries, vibrational frequencies, normal coordinates, and ADE calculated at the M06-2X/aug-cc-pVTZ level of theory. The predominantly excited vibrational modes of the neutral and the corresponding frequencies are also shown, where the ν_1 mode is C═O out-of-plane wagging vibration with a frequency of 40 cm^{-1}, and the ν_7, ν_{15}, and ν_{24} modes are noted in the text. The assignments in the stick spectra are specified in the legends, where each colored progression indicates a combination vibrational series.

To clearly exhibit contributions of different combination vibrations, Figure 4 shows the normal coordinate displacement vectors for each dominant vibrational mode when the ground-state neutral HFA is formed as well as their FCFs in the form of stick spectra. According to the fact that the C−O bond is shortened and the C−C bond is elongated (Figure 2) when the unpaired electron located in the anion HOMO is removed, two vibrations of neutral HFA, i.e., the C═O stretching mode (ν_{24} = 1946 cm^{-1}) and the carbon skeleton symmetric stretching mode (ν_{15} = 797 cm^{-1}), are expected to be predominantly activated. As shown in Figure 4, these two vibrational progressions are responsible for the experimental large difference of 0.64 eV between the VDE and ADE in the first band. Moreover, the C═O stretching mode (ν_{24} = 1946 cm^{-1}) agrees with the observed peak intervals (1895 ± 50 cm^{-1}) in the NIPE spectrum, indicative of the reliable modeling. Besides the two predominant vibrations of ν_{15} and ν_{24}, a few other vibrational modes are also probably excited in the electron detachment process, e.g., in-plane bending (ν_7 = 321 cm^{-1}), stretching (ν_9 = 479 cm^{-1}), and wagging (ν_{16} = 804 cm^{-1}) modes.

Similarly, the vibrational progressions associated with the Franck−Condon transitions from the anion to the triplet neutral (T_1) are calculated and shown in Figure 5. In comparison to the FCFs to the ground singlet neutral, a more complicated vibrational structure is predicted for the triplet band in the NIPE spectrum. Since both C−C bond

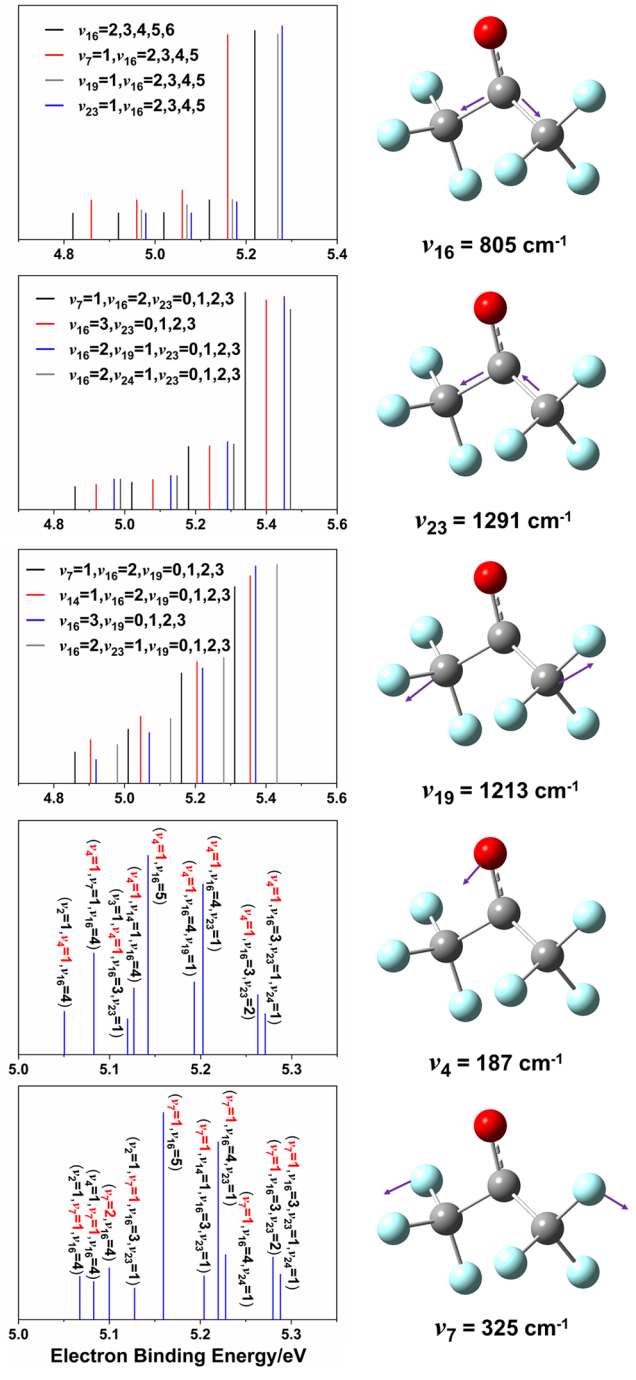

Figure 5. Calculated vibrational progressions (stick spectra) for the Franck−Condon transitions from $[HFA]^{\bullet-}$ to the triplet HFA neutral, using the optimized geometries, vibrational frequencies, normal coordinates, and ADE calculated at the M06-2X/aug-cc-pVTZ level of theory. The predominantly excited vibrational modes of the neutral and the corresponding frequencies are also shown. The assignments in the stick spectra are specified in the legends, where each colored progression indicates a combination vibrational series.

https://dx.doi.org/10.1021/acs.jpca.0c08996
J. Phys. Chem. A 2021, 125, 746−753

lengths are elongated and the C−C−C−F dihedral angle is evidently distorted, three vibrational modes of carbon skeleton symmetric stretching (ν_{16} = 805 cm^{-1}), asymmetric stretching (ν_{23} = 1291 cm^{-1}), and CF_3 wagging (ν_{19} = 1213 cm^{-1}) are predominantly excited during the removal of one electron from HOMO-1 of the anion, as displayed in Figure 5.

It is worth noting that the progressions of each sole carbon skeleton vibration are calculated with very weak intensities, and thus they are hardly visible in the calculated spectra. Interestingly, the C═O bending (ν_4 = 187 cm^{-1}) and C−F wagging vibration (ν_7 = 325 cm^{-1}) coupled with the carbon skeleton vibrations exhibit much stronger intensities, when we take into account more lower frequency vibrations associated with the C−C−C−F dihedral angle change by 27° from the equilibrium structure of the anion. Therefore, the calculated FCFs for these transitions strongly suggest a dense series of combination vibrational mode excitations in the electron photodetachment process from the ground-state anion to the triplet neutral.

3.4. Simulation of the NIPE Spectrum of [HFA]$^{\bullet-}$. Although partially resolved vibrational structures were observed in the NIPE spectrum, it is difficult to directly assign them due to overlapping of the combination vibrations and the broadened band profiles. Using the above FCFs, the 193 nm experimental NIPE spectrum of the [HFA]$^{\bullet-}$ radical anion was simulated. Figure 6 shows the comparison of the simulated and

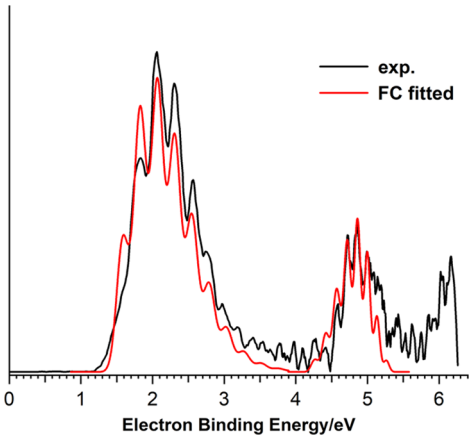

Figure 6. Experimental (in black) and simulated (in red) NIPE spectra at 193 nm, with a full width at half-maximum of 200 meV for the S_0 band and 80 meV for the T_1 band. To better match the experimental data, the calculated adiabatic detachment energies at the M06-2X level are slightly red-shifted by 0.13 eV for S_0 and 0.19 eV for T_1. The relative intensities of the convoluted vibrational progressions in the S_0 and T_1 bands were artificially adjusted to fit the experimental intensities.

experimental spectra with FWHM of 200 meV for the S_0 band and 80 meV for the T_1 band. To better match the experimental data, the calculated 0−0 origins (i.e., ADEs) of these two bands were slightly red-shifted, e.g., 0.13 eV for S_0 and 0.19 eV for T_1. Additionally, the relative intensities of the convoluted vibrational progressions in the S_0 and T_1 bands were artificially adjusted to fit the experimental intensities. Encouraged by the agreement in the rising edge of the S_0 band between the simulated and experimental spectra, we are highly confident that the obtained ADE is reliable. In other words, EA of HFA was experimentally determined to be 1.42 ± 0.02 eV. This agrees excellently with the previously estimated value of 1.43 eV from the gas-phase ion−molecule reactions by Chowdhury and McDonald.[36] As described in Section 3.3, the more complicated multiple vibrational excitations make it scarcely possible to discern every spectral characteristic in the T_1 band. Nevertheless, by fitting the T_1 band, the ADE of T_1 was similarly estimated to be 4.43 ± 0.02 eV, which is consistent with its theoretical values in Table 1.

Comparing the experimental (black) and simulated (red) spectra in Figure 6 clearly indicates that there exist extra spectral features at the right side of the T_1 band in the EBE range of 5.2−5.7 eV. As discussed above, they are provisionally assigned due to formation of the S_1 state for HFA, based on the good agreement between the observed EBEs with the calculated S_1 state positions. However, due to the poor signal-to-noise ratio in the region near the photon energy limit at 193 nm, vibrational structures in the S_1 state were not included in the simulation.

4. CONCLUSIONS

We measured the NIPE spectrum of the HFA$^{\bullet-}$ radical anion under the action of 193 nm photodetachment. There were two distinct broad bands in the 193 nm spectrum with a series of vibrational peaks. Using the M06-2X, PBE0, and ωB97XD density functionals with the aug-cc-pVTZ basis set, geometries and vibrational frequencies of the radical anion and the corresponding neutral were computed. Then, the Franck−Condon factors were calculated for electron detachments to produce neutral HFA in the ground singlet state and the lowest triplet state. Some combination vibrational modes, mainly including the C═O stretching and the carbon skeleton symmetric stretching, were suggested to be excited in the electron photodetachment due to significant geometrical changes, resulting in complicated vibrational progressions. Fortunately, satisfactory agreements were finally achieved for both bands between the experimental and calculated NIPE spectra. From the experimental and simulated spectra, the ADE and VDE of [HFA]$^{\bullet-}$ were determined to be 1.42 and 2.06 eV for formation of the neutral in the S_0 state and 4.43 and 4.86 eV for the T_1 state, respectively, providing the electron affinity of hexafluoroacetone of 1.42 ± 0.02 eV and adiabatic (vertical) singlet−triplet splitting of 3.01 (2.80) eV. These fundamental molecular properties, together with the obtained electronic configurations of HFA, are expected to provide useful information for investigations of its catalytic role in epoxidation reactions and stabilizing effect in detecting Criegee intermediates.

■ ASSOCIATED CONTENT

Supporting Information

The Supporting Information is available free of charge at https://pubs.acs.org/doi/10.1021/acs.jpca.0c08996.

Optimized geometry of the first electronically excited singlet state (S_1) of neutral HFA, calculated at the M06-2X/aug-cc-pVTZ level of theory (PDF)

■ AUTHOR INFORMATION

Corresponding Authors

Xiaoguo Zhou − *Hefei National Laboratory for Physical Sciences at the Microscale, Department of Chemical Physics, University of Science and Technology of China, Hefei 230026, Anhui, P. R. China;* orcid.org/0000-0002-0264-0146; Email: xzhou@ustc.edu.cn

https://dx.doi.org/10.1021/acs.jpca.0c08996
J. Phys. Chem. A 2021, 125, 746−753

Xue-Bin Wang − *Physical Sciences Division, Pacific Northwest National Laboratory, Richland, Washington 99352, United States;* orcid.org/0000-0001-8326-1780; Email: xuebin.wang@pnnl.gov

Authors

Lei Wang − *Hefei National Laboratory for Physical Sciences at the Microscale, Department of Chemical Physics, University of Science and Technology of China, Hefei 230026, Anhui, P. R. China*

Jia Han − *Hefei National Laboratory for Physical Sciences at the Microscale, Department of Chemical Physics, University of Science and Technology of China, Hefei 230026, Anhui, P. R. China*

Qinqin Yuan − *Physical Sciences Division, Pacific Northwest National Laboratory, Richland, Washington 99352, United States;* orcid.org/0000-0001-5771-6147

Wenjin Cao − *Physical Sciences Division, Pacific Northwest National Laboratory, Richland, Washington 99352, United States;* orcid.org/0000-0002-2852-4047

Shilin Liu − *Hefei National Laboratory for Physical Sciences at the Microscale, Department of Chemical Physics, University of Science and Technology of China, Hefei 230026, Anhui, P. R. China*

Complete contact information is available at: https://pubs.acs.org/10.1021/acs.jpca.0c08996

Author Contributions

[§]L.W. and J.H. contributed equally to this work.

Notes

The authors declare no competing financial interest.

■ ACKNOWLEDGMENTS

This work was supported by the U.S. Department of Energy (DOE), Office of Science, Office of Basic Energy Sciences, Division of Chemical Sciences, Geosciences, and Biosciences, and performed using EMSL, a national scientific user facility sponsored by DOE's Office of Biological and Environmental Research and located at Pacific Northwest National Laboratory, which is operated by Battelle Memorial Institute for the DOE. Financial support of the National Natural Science Foundation of China (Nos. 21873089 and 22073088), the Ministry of Science and Technology of China (No. 2012YQ220113), and the National Key Research and Development Program of China (No. 2016YFF0200502) is also gratefully acknowledged. The quantum chemical calculations were performed on the supercomputing system in the Supercomputing Center of the University of Science and Technology of China.

■ REFERENCES

(1) An, X. D.; Xiao, J. Fluorinated Alcohols: Magic Reaction Medium and Promoters for Organic Synthesis. *Chem. Rec.* **2020**, *20*, 142−161.

(2) Shuklov, I. A.; Dubrovina, N. V.; Boerner, A. Fluorinated Alcohols as Solvents, Cosolvents and Additives in Homogeneous Catalysis. *Synthesis* **2007**, *2007*, 2925−2943.

(3) Konno, T.; Iwashita, J.; Nagayama, K. Fluorinated Alcohol, The Third Group of Cosolvents that Stabilize the Molten-Globule State Relative to a Highly Denatured State of Cytochrome C. *Protein Sci.* **2000**, *9*, 564−569.

(4) Hoffmann, W.; Langenhan, J.; Huhmann, S.; Moschner, J.; Chang, R.; Accorsi, M.; Seo, J.; Rademann, J.; Meijer, G.; Koksch, B.; et al. An Intrinsic Hydrophobicity Scale for Amino Acids and Its Application to Fluorinated Compounds. *Angew. Chem., Int. Ed.* **2019**, *58*, 8216−8220.

(5) Altman, R. A. Fluorination and Fluorinated Compounds in Medicinal Chemistry. *Curr. Top. Med. Chem.* **2014**, *14*, 837−839.

(6) Fujiwara, T.; O'Hagan, D. Successful Fluorine-Containing Herbicide Agrochemicals. *J. Fluorine Chem.* **2014**, *167*, 16−29.

(7) Müller, K.; Boehm, H.-J. Facilitating the Design of Fluorinated Drugs. *Chem. Biol.* **2009**, *16*, 1130−1131.

(8) Müller, K.; Faeh, C.; Diederich, F. Fluorine in Pharmaceuticals: Looking beyond Intuition. *Science* **2007**, *317*, 1881−1886.

(9) Smart, B. E. Fluorine Substituent Effects (on Bioactivity). *J. Fluorine Chem.* **2001**, *109*, 3−11.

(10) Reichenbächer, K.; Suss, H. I.; Hulliger, J. Fluorine in Crystal Engineering - "The Little Atom that Could". *Chem. Soc. Rev.* **2005**, *34*, 22−30.

(11) Biswas, B.; Singh, P. C. The Role of Fluorocarbon Group in the Hydrogen Bond Network, Photophysical and Solvation Dynamics of Fluorinated Molecules. *J. Fluorine Chem.* **2020**, *235*, No. 109414.

(12) Narita, T. Synthesis of Novel Fluorinated Polymers: Facile Carbon-Carbon Bond Formation Aided by Fluorine Substituents. *Polym. J.* **2011**, *43*, 497−515.

(13) Wencel-Delord, J.; Colobert, F. A Remarkable Solvent Effect of Fluorinated Alcohols on Transition Metal Catalysed C-H Functionalizations. *Org. Chem. Front.* **2016**, *3*, 394−400.

(14) Liao, K. C.; Bowers, C. M.; Yoon, H. J.; Whitesides, G. M. Fluorination, and Tunneling across Molecular Junctions. *J. Am. Chem. Soc.* **2015**, *137*, 3852−3858.

(15) Heger, M.; Scharge, T.; Suhm, M. A. From Hydrogen Bond Donor to Acceptor: The Effect of Ethanol Fluorination on the First Solvating Water Molecule. *Phys. Chem. Chem. Phys.* **2013**, *15*, 16065−16073.

(16) Fukuhara, N.; Bigelow, L. A. The Action of Elementary Fluorine upon Organic Compounds. X. The Vapor Phase Fluorination of Acetone. *J. Am. Chem. Soc.* **1941**, *63*, 788−791.

(17) Janzen, A. F.; Rodesile, P. F.; Willis, C. J. Electrophilic Reactions of Hexafluoroacetone. *Chem. Commun.* **1966**, 672−673.

(18) Liu, Y.; Bayes, K. D.; Sander, S. P. Measuring Rate Constants for Reactions of the Simplest Criegee Intermediate (CH_2OO) by Monitoring the OH Radical. *J. Phys. Chem. A* **2014**, *118*, 741−747.

(19) Drozd, G. T.; Kroll, J.; Donahue, N. M. 2,3-Dimethyl-2-butene (TME) Ozonolysis: Pressure Dependence of Stabilized Criegee Intermediates and Evidence of Stabilized Vinyl Hydroperoxides. *J. Phys. Chem. A* **2011**, *115*, 161−166.

(20) Zaytsev, A.; Breitenlechner, M.; Novelli, A.; Fuchs, H.; Knopf, D. A.; Kroll, J. H.; Keutsch, F. N. Application of Chemical Derivatization Techniques Combined with Chemical Ionization Mass Spectrometry to Detect Stabilized Criegee Intermediates and Peroxy Radicals in the Gas Phase. *Atmos. Meas. Tech.* **2020**, DOI: 10.5194/amt-2020-335.

(21) Horie, O.; Schafer, C.; Moortgat, G. K. High Reactivity of Hexafluoro Acetone toward Criegee Intermediates in the Gas-Phase Ozonolysis of Simple Alkenes. *Int. J. Chem. Kinet.* **1999**, *31*, 261−269.

(22) Taatjes, C. A.; Welz, O.; Eskola, A. J.; Savee, J. D.; Osborn, D. L.; Lee, E. P. F.; Dyke, J. M.; Mok, D. W. K.; Shallcross, D. E.; Percival, C. J. Direct Measurement of Criegee Intermediate (CH_2OO) Reactions with Acetone, Acetaldehyde, and Hexafluoroacetone. *Phys. Chem. Chem. Phys.* **2012**, *14*, 10391−10400.

(23) Legros, J.; Crousse, B.; Bourdon, J.; Bonnet-Delpon, D.; Begue, J. P. An Efficient and Robust Fluoroketone Catalyst Epoxidation. *Tetrahedron Lett.* **2001**, *42*, 4463−4466.

(24) Legros, J.; Crousse, B.; Bonnet-Delpon, D.; Begue, J. P. Urea-Hydrogen Peroxide/Hexafluoro-2-Propanol: An Efficient System for a Catalytic Epoxidation Reaction without a Metal. *Eur. J. Org. Chem.* **2002**, *2002*, 3290−3293.

(25) van Vliet, M. C. A.; Arends, I.; Sheldon, R. A. Perfluoroheptadecan-9-One: A Selective and Reusable Catalyst for Epoxidations with Hydrogen Peroxide. *Chem. Commun.* **1999**, 263−264.

(26) Legros, J.; Crousse, B.; Bonnet-Delpon, D.; Begue, J. P. Design of Fluoroketones as Efficient Reagents for Epoxidation Reactions in Hexafluoropropan-2-ol. *Tetrahedron* **2002**, *58*, 3993−3998.
(27) Ganeshpure, P. A.; Adam, W. α-Hydroxy Hydroperoxides (Perhydrates) as Oxygen Transfer Agents in Organic Synthesis. *Synthesis* **1996**, *1996*, 179−188.
(28) Adam, W.; Degen, H. G.; Saha-Moller, C. R. Regio- and Diastereoselective Catalytic Epoxidation of Chiral Allylic Alcohols with Hexafluoroacetone Perhydrate. Hydroxy-Group Directivity through Hydrogen Bonding. *J. Org. Chem.* **1999**, *64*, 1274−1277.
(29) van Vliet, M. C. A.; Arends, I.; Sheldon, R. A. Hexafluoroacetone in Hexafluoro-2-Propanol: A Highly Active Medium for Epoxidation with Aqueous Hydrogen Peroxide. *Synlett* **2001**, *2001*, 1305−1307.
(30) Gandini, A.; Kutschke, K. O. Primary Process in Photolysis of Hexafluoroacetone Vapour. 2. Fluorescence and Phosphorescence. *Proc. R. Soc. London, A* **1968**, *306*, 511−527.
(31) Harland, P.; Thynne, J. C. J. Electron Attachment Cross Section for Hexafluoroacetone. *J. Phys. Chem. A* **1969**, *73*, 2791−2792.
(32) Harland, P.; Thynne, J. C. J. Positive and Negative Ion Formation in Hexafluoroacetone by Electron Impact. *J. Phys. Chem. B* **1970**, *74*, 52−59.
(33) Naff, W. T.; Cooper, C. D.; Compton, R. N. Electron Attachment and Excitation Processes in Selected Carbonyl-Compounds. *J. Chem. Phys.* **1972**, *57*, 1303−1307.
(34) Martin, I.; Langer, J.; Stano, M.; Illenberger, E. Reactions in Clusters of Acetone and Fluorinated Acetones Triggered by Low Energy Electrons. *Int. J. Mass Spectrom.* **2009**, *280*, 107−112.
(35) Szmytkowski, C.; Mozejko, P.; Ptasinska-Denga, E. Electron Scattering from Hexafluoroacetone Molecules: Cross Section Measurements and Calculations. *J. Phys. B* **2011**, *44*, No. 205202.
(36) McDonald, R. N.; Chowdhury, A. K. Gas-Phase Ion Molecule Reactions of Dioxygen Anion Radical ($O_2^{-\cdot}$). *J. Am. Chem. Soc.* **1985**, *107*, 4123−4128.
(37) Wang, L.; Yuan, Q. Q.; Cao, W. J.; Han, J.; Zhou, X. G.; Liu, S. L.; Wang, X. B. Probing Orientation-Specific Charge-Dipole Interactions Between Hexafluoroisopropanol and Halides: A Joint Photoelectron Spectroscopy and Theoretical Study. *J. Phys. Chem. A* **2020**, *124*, 2036−2045.
(38) Zhang, H. H.; Cao, W. J.; Yuan, Q. Q.; Zhou, X. G.; Valiev, M.; Kass, S. R.; Wang, X. B. Cryogenic "Iodide-Tagging" Photoelectron Spectroscopy: A Sensitive Probe for Specific Binding Sites of Amino Acids. *J. Phys. Chem. Lett.* **2020**, *11*, 4346−4352.
(39) Hou, G. L.; Wang, X. B. Spectroscopic Signature of Proton Location in Proton Bound $HSO4^{-}{\cdot}H^{+}{\cdot}X^{-}$(X = F, Cl, Br, and I) Custers. *J. Phys. Chem. Lett.* **2019**, *10*, 6714−6719.
(40) Wang, X. B. Cluster Model Studies of Anion and Molecular Specificities via Electrospray Ionization Photoelectron Spectroscopy. *J. Phys. Chem. A* **2017**, *121*, 1389−1401.
(41) Zeng, H. J.; Yang, N.; Johnson, M. A. Introductory Lecture: Advances in Ion Spectroscopy: From Astrophysics to Biology. *Faraday Discuss.* **2019**, *217*, 8−33.
(42) Dixon, A. R.; Khuseynov, D.; Sanov, A. Benzonitrile: Electron Affinity, Excited States, and Anion Solvation. *J. Chem. Phys.* **2015**, *143*, No. 134306.
(43) Hrovat, D. A.; Hou, G. L.; Chen, B.; Wang, X. B.; Borden, W. T. Negative Ion Photoelectron Spectroscopy Confirms the Prediction that D-3h Carbon Trioxide (CO_3) Has a Singlet Ground State. *Chem. Sci.* **2016**, *7*, 1142−1150.
(44) Chen, B.; Hrovat, D. A.; Deng, S. H. M.; Zhang, J.; Wang, X. B.; Borden, W. T. The Negative Ion Photoelectron Spectrum of meta-Benzoquinone Radical Anion ($MBQ^{-\cdot}$): A Joint Experimental and Computational Study. *J. Am. Chem. Soc.* **2014**, *136*, 3589−3596.
(45) Chen, B.; Hrovat, D. A.; West, R.; Deng, S. H. M.; Wang, X. B.; Borden, W. T. The Negative Ion Photoelectron Spectrum of Cyclopropane-1,2,3-Trione Radical Anion, $(CO)_3^{-\cdot}$ - A Joint Experimental and Computational Study. *J. Am. Chem. Soc.* **2014**, *136*, 12345−12354.
(46) Dauletyarov, Y.; Dixon, A. R.; Wallace, A. A.; Sanov, A. Electron Affinity and Excited States of Methylglyoxal. *J. Chem. Phys.* **2017**, *147*, No. 013934.
(47) Lineberger, W. C.; Borden, W. T. The Synergy between Qualitative Theory, Quantitative Calculations, and Direct Experiments in Understanding, Calculating, and Measuring the Energy Differences between the Lowest Singlet and Triplet States of Organic Diradicals. *Phys. Chem. Chem. Phys.* **2011**, *13*, 11792−11813.
(48) Lunny, K. G.; Benitez, Y.; Albeck, Y.; Strasser, D.; Stanton, J. F.; Continetti, R. E. Spectroscopy of Ethylenedione and Ethynediolide: A Reinvestigation. *Angew. Chem., Int. Ed.* **2018**, *57*, 5394−5397.
(49) Wenthold, P. G.; Hu, J.; Squires, R. R.; Lineberger, W. C. Photoelectron Spectroscopy of the Trimethylenemethane Negative Ion. The Singlet-Triplet Splitting of Trimethylenemethane. *J. Am. Chem. Soc.* **1996**, *118*, 475−476.
(50) Kregel, S. J.; Thurston, G. K.; Garand, E. Photoelectron Spectroscopy of Anthracene and Fluoranthene Radical Anions. *J. Chem. Phys.* **2018**, *148*, No. 234306.
(51) Schwarz, H.; Asmis, K. R. Identification of Active Sites and Structural Characterization of Reactive Ionic Intermediates by Cryogenic Ion Trap Vibrational Spectroscopy. *Chem. − Eur. J.* **2019**, *25*, 2112−2126.
(52) Lu, Z.; Continetti, R. E. Dynamics of the Acetyloxyl Radical Studied by Dissociative Photodetachment of the Acetate Anion. *J. Phys. Chem. A* **2004**, *108*, 9962−9969.
(53) Ichino, T.; Villano, S. M.; Gianola, A. J.; Goebbert, D. J.; Velarde, L.; Sanov, A.; Blanksby, S. J.; Zhou, X.; Hrovat, D. A.; Borden, W. T.; et al. The Lowest Singlet and Triplet States of the Oxyallyl Diradical. *Angew. Chem., Int. Ed.* **2009**, *48*, 8509−8511.
(54) Yuan, Q. Q.; Cao, W. J.; Wang, X. B. Cryogenic and Temperature-Dependent Photoelectron Spectroscopy of Metal Complexes. *Int. Rev. Phys. Chem.* **2020**, *39*, 83−108.
(55) Zhao, Y.; Truhlar, D. G. The M06 Suite of Density Functionals for Main Group Thermochemistry, Thermochemical Kinetics, Noncovalent Interactions, Excited States, and Transition Elements: Two New Functionals and Systematic Testing of Four M06-Class Functionals and 12 Other Functionals. *Theor. Chem. Acc.* **2008**, *120*, 215−241.
(56) Adamo, C.; Barone, V. Toward Reliable Density Functional Methods without Adjustable Parameters: The PBE0 Model. *J. Chem. Phys.* **1999**, *110*, 6158−6170.
(57) Chai, J. D.; Head-Gordon, M. Long-Range Corrected Hybrid Density Functionals with Damped Atom-Atom Dispersion Corrections. *Phys. Chem. Chem. Phys.* **2008**, *10*, 6615−6620.
(58) Frisch, M. J.; Trucks, G. W.; Schlegel, H. B.; Scuseria, G. E.; Robb, M. A.; Cheeseman, J. R.; Scalmani, G.; Barone, V.; Petersson, G. A.; Nakatsuji, H. et al. *Gaussian 16*, revision C.01; Gaussian, Inc.: Wallingford, CT, 2016.
(59) Mozhayskiy, V. A.; Krylov, A. I. ezSpectrum. http://iopenshell.usc.edu/downloads (accessed December 10, 2015).
(60) Reimers, J. R. A Practical Method for the Use of Curvilinear Coordinates in Calculations of Normal-Mode-Projected Displacements and Duschinsky Rotation Matrices for Large Molecules. *J. Chem. Phys.* **2001**, *115*, 9103−9109.

https://dx.doi.org/10.1021/acs.jpca.0c08996
J. Phys. Chem. A 2021, 125, 746−753